HHS Public Access

Author manuscript

Nat Immunol. Author manuscript; available in PMC 2013 June 01.

Published in final edited form as:

Nat Immunol. 2012 December ; 13(12): 1187–1195. doi:10.1038/ni.2449.

Mechanistic and structural insight into the functional dichotomy between interleukin-2 and interleukin-15

Aaron M. Ring[1,2], **Jian-Xin Lin**[3], **Dan Feng**[1,2], **Suman Mitra**[3], **Mathias Rickert**[1,2], **Gregory R. Bowman**[4], **Vijay S. Pande**[4], **Peng Li**[3], **Ignacio Moraga**[1,2], **Rosanne Spolski**[3], **Engin Özkan**[1,2], **Warren J. Leonard**[3], and **K. Christopher Garcia**[1,2]

[1]Howard Hughes Medical Institute, Stanford University School of Medicine, Stanford, California 94305, USA

[2]Department of Molecular and Cellular Physiology, and Department of Structural Biology, Stanford University School of Medicine, Stanford, California 94305, USA

[3]Laboratory of Molecular Immunology, National Heart, Lung, and Blood Institute, National Institutes of Health, Bethesda, MD 20892-1674, USA

[4]Department of Chemistry, Stanford University, Stanford, California 94720, USA

Abstract

Interleukin-15 (IL-15) and IL-2 possess distinct immunological functions despite both signaling through IL-2Rβ and the common cytokine receptor γ-chain, γ_c, We find that in the IL-15—IL-15Rα—IL-2Rβ—γ_c quaternary complex structure, IL-15 heterodimerizes IL-2Rβ and γ_c identically to the IL-2—IL-2Rα—IL-2Rβ—γ_c complex, despite differing receptor-binding chemistries. IL-15Rα dramatically increases the affinity of IL-15 for IL-2Rβ, and this allostery is required for IL-15 trans-signaling versus IL-2 cis-signaling. Consistent with the identical IL-2Rβ—γ_c dimer geometry, IL-2 and IL-15 exhibited similar signaling properties in lymphocytes, with any differences resulting from disparate receptor affinities. Thus, IL-15 and IL-2 induce similar signals, and the cytokine-specificity of IL-2Rα versus IL-15Rα determines cellular responsiveness. These results provide important new insights for specific development of IL-15- versus IL-2-based immunotherapeutics.

Correspondence should be addressed to K.C.G. (kcgarcia@stanford.edu).

ACCESSION CODES

Protein Data Bank (PDB): atomic coordinates and structure factors, 4GS7; Gene Expression Omnibus (GEO): IL-2 and IL-15 RNA-Seq data, GSE40350.

AUTHOR CONTRIBUTIONS

A.M.R., D.F., and E.Ö. performed crystallographic studies of the IL-15 quaternary complex. A.M.R. and E.Ö. determined and refined the structure. M.R. conducted SPR measurements. G.R.B. and V.S.P. conducted and analyzed molecular dynamics simulations. A.M.R. prepared cytokine proteins for signaling and transcriptional studies. A.M.R., S.M., I.M., and R.S. performed phosphoflow cytometry signaling experiments. A.M.R. conducted receptor internalization studies. J.X.L. and P.L. conducted and analyzed RNA-seq transcriptional assays and J.X.L. performed qPCR validation. A.M.R., J.X.L., G.R.B., W.J.L., and K.C.G. designed the experiments. A.M.R., J.X.L., P.L., S.M., and G.R.B. prepared the figures. A.M.R., W.J.L., and K.C.G. wrote the paper. W.J.L. and K.C.G. supervised the research.

Interleukin-15 (IL-15) and interleukin-2 (IL-2) are four-helix bundle cytokines critical to lymphocyte and natural killer (NK) cell function and homeostasis. Despite sparse sequence similarity (19% identity), both IL-2 and IL-15 heterodimerize IL-2Rβ and the common gamma chain, γ_c, to activate the Jak-STAT, PI3K-Akt, and Ras-MAPK pathways.[1] γ_c is additionally shared as a receptor component by IL-4, IL-7, IL-9, and IL-21 and is encoded by the gene mutated in humans with X-linked severe combined immunodeficiency (X-SCID)[2]. In accord with their use of common signaling receptors, IL-2 and IL-15 have several shared actions, such as stimulating cytotoxic T lymphocyte and NK cell proliferation and cytotoxicity[1]. However, these cytokines are not functionally redundant. IL-2 and IL-15 knockout mice have distinct phenotypes, and administration of IL-2 and IL-15 into mice and primates leads to divergent immunological outcomes[1,3]. While both cytokines stimulate diverse lymphocyte and natural killer subsets, IL-2 favors regulatory T cell homeostasis and the regulation of T helper (T_H) differentiation[4] whereas IL-15 favors expansion of CD8 memory cells, NK cells, and NK T cells[1].

The molecular basis for this paradox, namely, how IL-15 and IL-2 can signal through IL-2Rβ and γ_c but produce divergent functions, remains controversial. Both cytokines have private alpha-receptors, IL-2Rα (also known as CD25) for IL-2 and IL-15Rα for IL-15, which dramatically increase the sensitivity of each cytokine for the intermediate affinity receptor consisting of IL-2Rβ and γ_c[1]. Here, IL-15 is enigmatic in that it is dominantly presented in 'trans' by IL-15Rα to the IL-2Rβ and γ_c on a neighboring cell; whereas IL-2 can also be presented in trans[5], it is more typically presented in 'cis' to IL-2Rβ and γ_c on the same cell surface[6]. While neither IL-15Rα nor IL-2Rα are generally thought to possess signaling functions, this distinct mode of cytokine presentation to the signaling receptors could potentially explain some aspects of their different *in vivo* functions. Thus, explanations for the different functions of IL-2 and IL-15 could involve cis versus trans-presentation of the cytokines and/or the differential expression of their alpha receptors, coupled with unique temporal and spatial expression patterns of the cytokines themselves, resulting in selective stimulation of some cell types over others. An alternative conjecture is that IL-2 and IL-15 may produce fundamentally different signals, despite sharing common signaling receptors[7]. It is unclear from a structural perspective how IL-2 and IL-15 could transmit unique signals, although significantly divergent dimeric receptor topologies could, in principle, lead to different signaling outcomes, as has been speculated to occur for erythropoietin and other cytokines[8]. The crystal structure of the quaternary IL-2—IL-2Rα:IL-2Rβ:γ_c complex has been reported[9], as has the binary complex of IL-15 and IL-15Rα[10]. However, the absence of structural information for the complete quaternary IL-15 receptor ectodomain complex precludes conclusions about signaling differences arising from structural differences. The various hypotheses to explain distinct actions of IL-2 and IL-15, whether functionally or structurally derived, are not mutually exclusive, and the extent to which each contributes to the unique biological effects of IL-2 and IL-15 is unclear.

In this report, we investigated several aspects of IL-15 structural and functional biology. First, we determined the crystal structure of the IL-15 quaternary complex in order to compare the molecular recognition strategies employed by IL-15 and IL-2 in binding the

shared IL-2Rβ and γ_c receptors, as well as to assess the relative geometries of receptor heterodimerization induced by the two cytokines. Second, informed by these structural comparisons, we conducted molecular dynamics simulations and biophysical affinity measurements to probe the mechanism whereby IL-15Rα enhances IL-15 potency. Finally, in light of the structural data pointing to highly similar receptor-binding modes, we characterized the signaling and gene expression profiles of lymphocytes induced by IL-2 and IL-15 to assess whether these cytokines produce different intracellular signals that could explain their functional differences.

RESULTS

Comparison of the IL-15 and IL-2 quaternary complexes

Our initial attempts to determine the structure of the quaternary complex of IL-15 yielded crystals that diffracted to a resolution of only 3.8Å. To obtain a higher-resolution structure, we performed reductive methylation of the complex. This mild chemical modification results in di-methylation of surface lysines that can often improve crystal diffraction[11], and in this manner we improved diffraction of the IL-15 quaternary receptor complex to 2.35 Å (Table 1; Supplementary Fig. 1a–c, Supplementary Fig. 2a). We determined the structure by molecular replacement using models of IL-2Rβ, γ_c, IL-15 and IL-15Rα previously reported[9,10]. The overall structure of the IL-15 quaternary complex (Fig. 1a) bears close similarity to the two other γ_c cytokine receptor complexes reported so far, containing IL-2 and IL-4[9,12]. The IL-15 quaternary complex, containing its private alpha-receptor and the shared signaling receptors IL-2Rβ and γ_c, assembles in a nearly identical fashion as the IL-2 quaternary complex (Fig. 1b left, PDB code 2B5I), with IL-2Rβ binding to “site I” and γ_c to “site II” on the cytokine. The structures of the IL-15 and IL-2 quaternary complexes can be superimposed with a root-mean-square deviation RMSD of 1.18 Å, indicating close structural similarity (Fig. 1b right). In the signaling subunits IL-2Rβ and γ_c, the greatest differences between the IL-2 and IL-15 complexes reside in slight repositioning of the D1 domains contacting the cytokines. By contrast, the positions of the D2 domains, which form the receptor-receptor contacts and lead towards the cell surface, are nearly identical, suggesting that functional differences between IL-2 and IL-15 signaling are unlikely to be explained by alteration of the receptor architecture or dimer-angle geometry.

At the IL-2Rβ site I interface (Fig. 2a and b), IL-15 and IL-2 share sparse identity, with only three contact residues conserved (D8, D61, and N65 of IL-15; D20, D84, and N88 of IL-2) among the fifteen residues that contact IL-2Rβ (Fig. 2c). In an example of convergent structural evolution, these three residues are not conserved in linear sequence, but rather in their three-dimensional spatial locations on the cytokine helices forming the receptor-binding interface (Fig. 2c). They make identical contacts with IL-2Rβ: D8 forms hydrogen bonds to H133 and Y134 of IL-2Rβ; D61 forms a salt-bridge with K71; and N65 contacts the triad of R42, Q70, and Y134. The significance of these residues has been confirmed by mutagenesis studies for both IL-2 and IL-15[13–16]. Of the remaining site I contact residues in IL-15, many are relatively conservative substitutions to IL-2, and interact with IL-2Rβ in a similar fashion. For example, V91 and I92 of IL-2 form van der Waals interactions with T73 and V75 of IL-2Rβ; in IL-15, the same contacts are made by I68 and L69. However, there

are some striking differences in the binding chemistry of the IL-2—IL-2Rβ and IL-15—IL-2Rβ interfaces. IL-2 recognizes E136 of IL-2Rβ through a hydrophobic interaction between L19 and the aliphatic portion of the glutamic acid side chain (Fig. 2b). In the IL-15 site I interface, this interaction takes a completely different character as E136 forms a hydrogen bond with S7 of IL-15 (Fig. 2a). Another salient feature of the IL-15—IL-2Rβ interaction is the lysine pair K10 and K11. K10 forms a salt-bridge with E136 of IL-2Rβ that has no equivalent in IL-2, while K11 appears to satisfy the role that two IL-2 residues play at the site I interface. Pointing upward from helix A toward helix C, K11, like M23 of IL-2, presents the aliphatic portion of its side-chain for van der Waals interactions with H133 of IL-2Rβ, while positioning its terminal amine at the same site as the guanidinium of IL-2's R81 (Fig. 2a–c). Thus, while the three key contact residues in the interface are maintained between IL-2 and IL-15, the overall divergence of the IL-2Rβ binding chemistry clearly suggests that cytokine-specific strategies to disrupt or enhance IL-2 versus IL-15 binding is feasible in an engineered protein therapeutic.

Despite the sequence dissimilarity and the unique binding strategies of IL-2Rβ's ligands IL-2 and IL-15, the conformation of the side chains and binding loops of IL-2Rβ are nearly indistinguishable when complexed to either cytokine. Of the 14 residues contacting either IL-2 or IL-15, only two residues show substantial changes in position or rotameric conformation (Fig. 2d). The apparent rigidity of the IL-2Rβ interface despite cross-reactivity to multiple cytokines is reminiscent of the shared cytokine receptor gp130, and suggests that like gp130, the mechanism of degenerate cytokine recognition by IL-2Rβ is not driven by conformational plasticity[17]. Rather, the receptor appears to have evolved a rigid interface that accommodates diverse energetic binding solutions, reminiscent of other cross-reactive immune receptors such as NKG2D[18].

At its site II interface, IL-15 binds to γ_c through a rather chemically 'featureless' interface that stands in stark contrast to the highly polar and specific side chains contacts seen in the site I interface. Although the IL-15 interaction does exhibit some unique features, a similar docking strategy is used for γ_c binding to IL-2 and IL-4, and this highlights the cross-reactive properties of the γ_c cytokine-binding surface, which has the capacity to engage all of the γ_c-cytokine family members. In particular, the absence of highly charged bonds would facilitate degenerate cytokine binding. Like IL-2 and IL-4 (not shown), IL-15 interacts with the EF1, BC2, and FG2 loops of γ_c by side-chains positioned by the A and D helices (Fig. 3a and b). In a similar example of three-dimensional structural mimicry as seen in site I, the most critical hotspot residue Q126 of IL-2 is conserved in IL-15 as Q108 and packs neatly into the same trench of γ_c that is formed by residues P207, C209, G210, and S211. Similarly, Y103 of $\gamma_{c,}$ which is mutated in some individuals with X-SCID and appears critical for optimal ligand binding, is satisfied by parallel mechanisms in IL-2 and IL-15; the phenyl ring packs with S127 of IL-2 and M109 of IL-15, while the hydroxyl moiety makes a hydrogen-bond to IL-2 S130 and IL-15 N112.

IL-15 is smaller than IL-2 (108 versus 133 residues) and a distinct structural feature in site II appears to have evolved to compensate for this difference. In the IL-15 site II interface, there is an additional region of contact between residues on the A-B loop of IL-15 and the CC′1 loop of γ_c (Fig. 3a, c, and d). This interface buries an area of 490 $Å^2$, which constitutes over

one third of the entire buried surface area (BSA) of the IL-15 site II interface (1367 Å^2). IL-2 forms a much smaller interface with this region of γ_c, contributing only 70 Å^2 or 7% of a total site II BSA of 995 Å^2 (Fig. 3d). IL-15 has shorter A and D helices than IL-2 (two and 1.5 turns shorter, respectively), and consequently makes fewer contacts to γ_c from these helices. While IL-2 has 10 contact residues located between these two helices, IL-15 has only five. Furthermore, IL-15 binds to γ_c with considerably lower shape complementarity than IL-2 or IL-4 (sc=0.59 for IL-15 versus 0.84 for IL-2 and 0.82 for IL-4). Thus, a potential explanation for IL-15's unique contacts to the γ_c CC'1 loop is that the interface serves to have compensated for the missing A and D helical contacts present in other γ_c cytokines as well as IL-15's less favorable shape complementarity with γ_c.

In conclusion, IL-15 assembles the IL-2Rβ—γ_c signaling complex in a fashion nearly indistinguishable from IL-2, despite both shared and unique molecular recognition strategies in binding the receptor subunits. The great overall similarity of the IL-15 and IL-2 complexes' structures disfavors structural explanations for the unique functional properties of the cytokines. However, the details of the cytokine and receptor contacts present structural opportunities for the specific disruption or enhancement of either cytokine for therapeutic purposes.

Molecular insight into IL-15 trans-signaling

Signaling through the IL-2 and IL-15 receptors is initiated when IL-2Rα or IL-15Rα captures IL-2 or IL-15, respectively, and presents the cytokine to IL-2Rβ and γ_c. IL-15, however, can signal through an unusual mechanism whereby it is presented *in trans* by cells expressing IL-15 and IL-15Rα to IL-15-responsive cells expressing IL-2Rβ and γ_c[19]. Unlike the situation *in cis*, IL-15 trans-signaling does not benefit from the substantial surface-capture effect of IL-15Rα binding to IL-15 on the same cell, as is the case for IL-2. A major role for IL-2Rα is simply to enrich the cell surface by capturing IL-2 from solution, which results in a dramatic reduction in the entropic barrier for IL-2 binding to IL-2Rβ and γ_c. Since IL-15 is presented *in trans*, it does not enjoy this mechanistic advantage, raising the question of how IL-15Rα effectively enhances IL-15 activity. Nevertheless, trans-presentation has proven to be a major mechanism of IL-15 action *in vivo*[6], suggesting that IL-15Rα may have other IL-15 sensitizing functions in addition to surface capture. We and others have found that IL-15 in complex with soluble IL-15Rα has greater biological activity than does free IL-15 on some cell types[20–22]. Salient to this point is that previously we observed that IL-2 undergoes a small conformational change upon binding to IL-2Rα in the region of the IL-2 C-helix contacting IL-2Rβ[23]. Furthermore, mutant IL-2 superkines (e.g., "Super-2" or "H9") that stabilize the C-helix enhance IL-2's affinity for IL-2Rβ by nearly 300-fold[24]. Since IL-15 would not benefit from the entropic gain resulting from cis surface capture by IL-15Rα, as does IL-2, we sought to determine to what extent IL-15Rα induces an affinity enhancement of IL-15 for IL-2Rβ through trans capture and presentation. We performed surface plasmon resonance affinity measurements of both free and IL-15Rα-bound IL-15 for immobilized IL-2Rβ. Free IL-15 bound to IL-2Rβ with a K_D of 438 nM (Fig. 4a left), consistent with prior SPR measurements for this interaction[25]. Interestingly, IL-15—IL-15Rα complex bound to IL-2Rβ with a K_D of 3 nM (Fig. 4a right), an affinity increase of approximately 150-fold over free IL-15.

The structure of the quaternary IL-15 complex does not offer an obvious explanation for how IL-15Rα influences the interaction between IL-15 and IL-2Rβ. Notably, IL-15Rα does not contact IL-2Rβ, with a distance of >15Å separating the subunits at their closest point (Fig. 4b). However, the conformational mechanisms of this allostery may be dynamic and subtle, and likely not observable in a static crystal structure. Structural alignment of the binary (PDB: 2Z3Q) and quaternary IL-15 complexes indicates that the IL-15—IL-15Rα complex does not undergo a significant conformational change upon binding IL-2Rβ and γ_c (RMSD 0.453Å; Supplementary Fig. 2b). Therefore, we hypothesized that IL-15Rα might thus stabilize a conformation of IL-15 that is more competent to bind IL-2Rβ, akin to the effect of IL-2Rα for IL-2. A direct comparison between free and IL-15Rα-bound IL-15 is not currently possible, as the structure of free IL-15 has yet to be elucidated, likely owing to the biochemical instability of the molecule in the absence of IL-15Rα[20]. We instead turned to computational approaches to interrogate the potential structural and dynamics influences of IL-15Rα on IL-15.

Proteins exist in solution as flexible conformational ensembles whose equilibrium can be perturbed upon ligand binding. For example, IL-2 has been shown to be highly conformationally-plastic[26]. Using molecular dynamics (MD) simulations, we asked how binding to its alpha-receptor alters the conformational ensemble of IL-15. We constructed an atomically detailed Markov state model (MSM) in order to directly probe the relative conformational flexibility of IL-15 when free in solution or when bound to alpha-receptor. The states in this MSM come from kinetic clustering of rapidly inter-converting conformations resulting from atomistic simulations[27]. Each of these metastable states corresponds to a local minimum in the underlying free energy landscape that ultimately determines the system's structure and dynamics. Using these MSMs, we calculated the average RMSD for each structural element under the two conditions (Fig. 4c). This analysis reveals that the conformational freedom of the A-B and C-D loops is greatly restricted in the bound state, which is expected, given that these loops form the contacts to IL-15Rα. To a lesser extent, there appears to be global stabilization of the four helices. Visualization of the most highly populated conformations from each set of conditions shows that the differences are subtle, both in the helices and loops (Fig. 4d). This is a notable contrast to IL-2, where binding of IL-2Rα specifically repositions the B and C helices of IL-2 for optimal binding to IL-2Rβ[23,24]. Despite these disparate mechanisms—global versus helix-specific stabilization—our results suggest that IL-15Rα and IL-2Rα share the property of conformationally-stabilizing relatively flexible cytokine ligands, in order to decrease energetic barriers to binding and increase affinity of IL-15 and IL-2 for IL-2Rβ.

Comparison of IL-15 and IL-2 signaling properties

There is considerable controversy whether IL-2 and IL-15 yield different intracellular signals upon receptor activation. While some investigators have found that the cytokines give indistinguishable signaling profiles[28], others have demonstrated significant differences. These differences have been reported to be alterations in signaling kinetics[29,30] and efficacy[31] for individual pathways. Given the great structural similarity between the quaternary complexes of IL-2 and IL-15, we sought to re-examine their membrane-proximal signaling activities. To this end, we determined the dose-response relationships and

signaling kinetics of IL-2 and IL-15 on cells expressing or deficient of IL-2Rα and IL-15Rα. We took advantage of the NK cell line YT-1, which we sorted into separate IL-2Rα+ and IL-2Rα− subpopulations (Supplementary Fig. 3a), for dose-response and kinetic analysis of STAT5 and ERK phosphorylation as assayed by phosphoflow cytometry (Fig. 5). We also isolated CD8 T cells from mouse spleens and assayed phosphorylation of STAT5 and S6 kinase (a component of the PI3K signaling pathway) in response to cytokine application for freshly-isolated cells and cells pre-stimulated with anti-CD3 antibody (Fig. 6). Whereas pre-stimulated CD8 cells expressed both alpha-receptors at moderate to high levels, freshly-isolated CD8 cells did not express IL-2Rα and expressed only a modest level of IL-15Rα (Supplementary Fig. 3b). To further isolate alpha-receptor mediated effects, we performed our experiments using IL-15—IL-15Rα complexes and H9, an IL-2 "superkine" with high affinity for IL-2Rβ such that it can potently induce signaling through the IL-2Rβ—γ_c heterodimer on IL-2Rα-negative cells, in addition to free IL-15 and wild-type IL-2[24].

On YT-1 cells lacking IL-2Rα, the respective signaling EC_{50} for each cytokine correlated with its relative affinity for IL-2Rβ, with the rank order for EC_{50}'sbeing IL-15—IL-15Rα = H9 < IL-15 < IL-2 (Fig. 5, top left). The somewhat lower EC_{50} of IL-15 compared to IL-2 likely results from the small amount of IL-15Rα expressed on YT-1 cells (Supplementary Fig. 3a). When IL-2Rα was present, the EC_{50} rank order was H9 = IL-2 < IL-15—IL-15Rα < IL-15, reflecting surface-capture and avidity effects of membrane-bound IL-2Rα on IL-2 and H9 (Fig. 5, top right). We observed similar results when comparing the dose-response relationships derived from freshly-isolated and pre-activated mouse CD8 cells, but with a few distinctions. On freshly-isolated CD8 cells, free IL-15 produced a biphasic dose-response relationship, consistent with the low level of expression of IL-15Rα in these cells, including a high proportion of cells negative for the receptor (Fig. 6, top left; Supplementary Fig. 3b). Notably, IL-15—IL-15Rα complexes did not demonstrate a biphasic dose-response curve as the presence of soluble IL-15Rα likely impeded engagement of membrane-bound IL-15Rα. The subsequent rank order of EC_{50}'s was IL-15$EC_{50\#1}$ < H9 < IL-15—IL-15Rα< IL-15$EC_{50\ \#2}$ = IL-2. On pre-activated CD8 cells, the EC_{50}'s of IL-2 and IL-15 dramatically shifted to the left, reflecting the potent effect of IL-2Rα and IL-15Rα expression on cytokine sensitivity (Fig. 6, top right). H9 also shifted to the left as it is competent to bind IL-2Rα and benefits from surface-capture, but the EC_{50} of the IL-15—IL-15Rα complex was essentially unchanged compared to freshly-isolated cells. For all cells and irrespective of differences in EC_{50}, IL-2, H9, and IL-15—IL-15Rα complex stimulated equivalent levels of STAT5, ERK, and pS6 kinase phosphorylation at saturating doses.

We proceeded to monitor the kinetics of IL-2 and IL-15 signaling using sub-saturating (1 nM or 20 pM) and saturating doses (500 nM or 10 nM) of IL-2, H9, IL-15, and IL-15—IL-15Rα complexes. We assayed the three major IL-2 and IL-15 signaling pathways—Jak-STAT, Ras-MAPK, and PI3K-Akt—and found their signaling kinetics to be highly concentration and alpha-receptor dependent (Figs. 5 and 6, 2nd and 3rd rows). In particular, both the rate and magnitude of signaling for each pathway was readily predicted by their respective concentration-response relationships. For instance, at sub-saturating concentrations and in the absence of IL-2Rα, IL-2 demonstrated the slowest signaling kinetics compared to the other cytokines, matching its right-shifted dose-response curve under those conditions (Figs. 5 and 6, 1st column). A similar trend is seen for IL-15—

IL-15Rα complexes on pre-activated cells at sub-saturating conditions (Figs. 6, 3rd column). By contrast, all four stimuli produced overlapping and nearly-identical kinetic profiles of STAT5, ERK, and S6kinase phosphorylation at saturating cytokine concentrations (Figs. 5 and 6, 2nd and 4th columns). Consistent with STAT5, ERK, andS6kinase phosphorylation, downregulation of the signaling receptor IL-2Rβ also demonstrated a strong relationship with cytokine affinity and concentration (Fig. 5, bottom row). Specifically, the higher affinity cytokines drove faster and more complete IL-2Rβ internalization at lower cytokine concentrations, but the differences were diminished at saturating doses. Taken together, these results indicate that IL-2 and IL-15 generate highly similar, if not identical, intracellular signals after accounting for variability in alpha-receptor expression and cytokine receptor affinity.

IL-2 and IL-15 produce similar gene expression profiles

As with intracellular signaling, differences in gene expression induced by IL-2 and IL-15 have been reported[31,32], perhaps accounting in part for functional differences between the two cytokines. We wondered if these differences, like the reported differences in membrane-proximal signaling, could be explained by concentration-dependent effects, or if the two cytokines produce fundamentally different gene expression profiles. To maximize our chances of detecting genes differentially-regulated between IL-2 and IL-15, we compared gene expression profiles using RNA-Seq in $CD8^+$ T cells stimulated with sub-saturating cytokine concentrations (1 nM) commonly used by other investigators in the field, or saturating concentrations (500 nM) of each cytokine. A two-dimensional multidimensional scaling (MDS) plot analysis showed that IL-2-and IL-15-regulated mRNAs correlated at each time point and concentration (Supplementary Fig. 4a). As seen with membrane-proximal signaling induced by IL-2 and IL-15, the gene expression profiles of the cytokines were most similar when the cytokines were applied at saturating concentrations (R^2=0.909 and 0.962 at 4 and 24 hours, respectively; Fig. 7a bottom panels) than at sub-saturating concentrations (R^2=0.784 and 0.611 at 4 and 24 hours, respectively; Fig. 7a top panels). To identify IL-2- and IL-15-regulated mRNAs, we chose those mRNAs with RPKMs (Reads Per Kilobase of exon model per Million mapped reads) > 5 that exhibited a fold change in expression ≥ 2 at any time point as compared to the unstimulated control. This analysis identified 4,690 mRNAs regulated by IL-2 and 4,776 mRNAs regulated by IL-15; many of the same genes were regulated by both cytokines so that a total of 5182 different mRNAs were regulated by at least one of these cytokines (Supplementary Fig. 4b). 90.5% of IL-2-regulated mRNAs and 92.2% of IL-15-regulated mRNAs were expressed at similar levels following IL-2 or IL-15 stimulation (i.e., the difference in the fold change between IL-2 and IL-15 at the same time point was < 2). By contrast, 406 mRNAs were more potently regulated by IL-2 than by IL-15 (ratio of expression levels stimulated by IL-2 vs IL-15 >2), and 492 mRNAs were more potently regulated by IL-15 than by IL-2 (Fig. 7b–d; Supplementary Fig. 4b; Supplementary Spreadsheet 1 and 2).

Having identified candidate genes that may be differentially-regulated by IL-2 and IL-15, we sought to validate the gene expression differences and determine if they persisted independently of concentration. Thus, we performed RT-qPCR of $CD8^+$ T cells that were stimulated with sub-saturating (1 nM) or saturating (500 nM) concentrations of each

cytokine and assayed for gene expression for a set of genes at early (4 hr) and late (24 hr) time points. As we observed in our RNA-seq experiments, at 1 nM, IL-2 and IL-15 produced statistically-significant differences in gene expression at both time points (Fig. 8a–c). However, when we applied saturating concentrations of each cytokine, the expression levels converged for most of the genes assayed (Fig. 8a and c). Some differences persisted at high concentration, as IL-2 induced greater expression of *Il2ra, Tnf*, and *Ifng* than did IL-15 even at high concentration (Fig. 8b). These differences were relatively modest, however, ranging from less than 0.5 fold for *Tnf* to approximately three-fold for *Ifng*. Thus, paralleling their membrane-proximal signaling behavior, IL-15 and IL-2 stimulate highly similar transcriptional profiles, particularly when accounting for cytokine concentration and alpha-receptor expression.

DISCUSSION

Since the initial discovery of IL-15 almost 20 years ago, numerous mechanisms have been offered to explain how IL-2 and IL-15 can produce divergent functional effects despite sharing common signaling receptors. In this work, we report the x-ray crystal structure of the quaternary complex of IL-15 bound to the ectodomains of IL-15Rα, IL-2Rβ, and γ_c and find the complex to have an approximately identical heterodimeric IL-2Rβ—γ_c architecture to that of the IL-2—IL-2R quaternary complex. The lack of significant deviations in dimer topology between the signaling complexes of IL-2 and IL-15 suggest that any functional differences between the two cytokines are unlikely to arise from instructive extracellular structural influences. However, differences in the cytokine interaction affinities and kinetics of the respective cytokine associations with the IL-2Rβ and γ_c extracellular domains could result in overall complex stability differences that would be manifested as distinct signaling outcomes. Thus, using phospho-flow cytometry, we compared IL-2 and IL-15 mediated signaling over a broad range of cytokine concentrations and kinetic intervals, finding that many of the apparent signaling differences between IL-2 and IL-15 may be explained by differences in receptor affinity between the two cytokines. Similarly, we found the gene expression profiles of cells stimulated with IL-2 and IL-15 to be highly correlated and that differences in gene expression were generally diminished at saturating concentrations of the cytokines. When differences persisted at saturation, they remained modest, bringing into question their true biological relevance. While our results do not rule out the possibility of additional mechanisms of IL-15 action, they indicate these mechanisms are not necessary to explain the complex and diverse functional behaviors of IL-15 and IL-2 observed *in vivo*. Rather, we find that alpha-receptor expression and cytokine concentration drastically affect the signaling behavior of IL-2 and IL-15, producing differences in gene expression when the cytokines lie at different points on their respective concentration-response curves. Presumably, the disparate spatial and temporal expression of the alpha receptors, as well as their absolute expression level, dynamically regulates the sensitivity of cells for each respective cytokine and their ensuing response to stimulation.

Underscoring the importance of their respective alpha receptors in their functions, a striking difference between IL-2 and IL-15 can be seen in the manner in which the cytokines are presented to effector cells. Since IL-15 binds to IL-15Rα with an extremely high affinity and IL-15Rα is widely expressed in tissues, IL-15 is believed to mainly exist in the body as a

complex with IL-15Rα, and is therefore primed for trans-presentation to cells expressing IL-2Rβ and γ_c[6]. As previously mentioned, soluble complexes of IL-15—IL-15Rα mimicking trans-presentation show enhanced potency compared to free IL-15[20–22]. Through our studies, we elucidated the mechanism underlying this phenomenon, finding that binding of IL-15Rα increases the affinity of IL-15 for IL-2Rβ approximately 150-fold. This affinity increase for IL-2Rβ subsequently manifests as a left-shift in the concentration-response relationship of IL-15 signaling in cells lacking IL-15Rα. The structural basis for the affinity enhancement of IL-15 for IL-2Rβ appears to be a consequence of a global stabilization of IL-15 upon binding IL-15Rα to a much greater degree than seen for IL-2 upon binding IL-2Rα[23,24]. From a teleological perspective, the affinity enhancement endowed by IL-15Rα onto the IL-15—IL-2Rβ interaction may serve to compensate for the lack of surface-capture in the setting of trans-presentation.

IL-2 is administered clinically as immunotherapy in the treatment of renal cell carcinoma and metastatic melanoma. However, IL-2 therapy is hampered by dose-limiting toxicity from vascular leakage and the counter-productive activation of regulatory T cells (Treg) that abrogate anti-tumor responses. Both of these undesirable side-effects are attributable to the activation of cells that express IL-2Rα: pulmonary vascular endothelial cells and IL-2Rα$^+$, CD4$^+$ Treg cells[33,34]. Recently, we demonstrated that IL-2 variants that bind to IL-2Rβ with high affinity independently of IL-2Rα (“Super-2” or “H9”) produce greater anti-tumor efficacy and decreased pulmonary edema compared to wild-type IL-2[24]. Compared to wild-type IL-2, Super-2 more efficiently activates anti-tumor responses from IL-2Rα$^-$ cells such as naive T cells and NK cells, with proportionally less activation IL-2Rα$^+$ cells such as Treg and pulmonary endothelial cells. In recent years, the potential use of IL-15 for the treatment of cancer has garnished considerable enthusiasm and it is presently undergoing evaluation in phase I clinical trials (ClinicalTrials.gov identifier NCT01021059). Notably, IL-15 does not produce vascular leak syndrome or stimulate Treg, but preferentially activates cytotoxic T lymphocytes and NK cells thought to mediate anti-tumor effects[3], in many ways similar to Super-2. Similarly, a single-chain fusion protein of IL-15 and IL-15Rα (RLI) has been proposed as a potential anti-tumor agent, with enhanced potency and bioavailability compared to free IL-15[35].

In comparing the therapeutic anti-tumor potential of IL-2, IL-15, and their respective variants, Super-2 and IL-15—IL-15α complexes, it is important to consider the degree of alpha-receptor dependence inherent to each molecule. While IL-2 and IL-15 represent the extreme ends of the spectrum, showing great dependence on their alpha-receptors for potency, Super-2 and the single-chain IL-15—IL-15Rα fusion RLI appear to lie in-between the two wild-type cytokines, showing little to no preference for cells expressing IL-2Rα or IL-15Rα. Super-2 and RLI can be further distinguished by their interactions with IL-2Rα and IL-15Rα. Since the IL-15Rα binding site is sterically-obscured in RLI, it represents the exact midpoint between IL-2 and IL-15 on the spectrum, unaffected by the presence or absence of either alpha-receptor. By contrast, Super-2 is capable of binding IL-2Rα and subsequently shows some preference for IL-2Rα$^+$ cells over IL-2Rα$^-$ cells, albeit at a much-decreased degree than wild-type IL-2. This subtle distinction may yield important differences in efficacy and toxicity. For example, though IL-2Rα is responsible for many of IL-2’s undesirable side effects, some IL-2Rα$^+$ cells may be beneficial to target, such as

activated T cells. Similarly, IL-15Rα$^+$ cells such as NK and cytotoxic CD8 cells are critical determinants of anti-tumor efficacy *in vivo*.

In light of these considerations, it may be possible to enhance IL-2 and/or IL-15 immunotherapy by modulating their dependencies on IL-2Rα and IL-15Rα, respectively, thus "tuning" the distribution of immune cells activated for therapeutic effect. To this end, Super-2 and RLI represent good starting points for such immunological manipulation. Just as the structure of the IL-2 quaternary complex enabled the engineering of Super-2, we hope to leverage the information from the IL-15 quaternary complex presented here for the design of improved IL-15 therapies.

ONLINE METHODS

Protein expression and purification

For crystallization, human IL-15 (1-114)-6xH in pET22b and human IL-15Rα (1-67)-6xH in pET26b were co-expressed in the periplasm of BL21(DE3) cells by induction with IPTG for 20 hours at 22°C. Periplasmic fraction was isolated by osmotic shock and recombinant protein was purified by Ni-NTA chromatography followed by size-exclusion chromatography with a Superdex-75 column into HBS (10 mM HEPES pH 7.4, 150 mM NaCl, 0.02% sodium azide). Human IL-2Rβ (1–214) with Asn residues 3, 17, 45 mutated to Gln and human γ_c (34–232) with Asn53 mutated to Gln were expressed and purified from Hi5 cells as previously described[9]. Purified, *E. coli*-derived IL-15—IL-15Rα complex was then mixed with purified, insect-derived IL-2Rβ and γ_c at a 1:1:1 ratio and treated with carboxypeptidases A and B overnight at 4°C. The digested proteins were then methylated as previously described [11] and purified by size-exclusion chromatography with a Superdex-200 column into HBS.

For signaling and SPR experiments, IL-15 (1–114) and IL-15 co-expressed with IL-15Rα (1–64) were produced in Hi5 cells and purified by Ni-NTA and size-exclusion chromatography. Biotinylated IL-2Rβ was obtained by addition of a C-terminal biotin acceptor peptide (BAP) tag (GLNDIFEAQKIEWHE) and co-expression with BirA ligase with excess biotin (100μM) added to the expression media. Human IL-2 (1–133) and high-affinity variant H9 were expressed and purified from Hi5 cells as previously described[24].

Crystallization and Data Collection

Purified, carboxypeptidase-treated, methylated IL-15—IL-15Rα—IL-2Rβ—γ_c quaternary complex was concentrated to 12.1 mg/mL and crystallized by vapor diffusion in hanging-drops by addition of 0.1μL mother liquor (22.5% PEG3350, 0.1M BIS-TRIS propane pH 8.75, 0.2M sodium acetate) to 0.1μL protein. Crystals grew to a maximum size of 150×50×50 μm after 2–3 days at 22°C. Crystals were cryoprotected in motherliquor supplemented with 15% ethylene glycol and flash frozen in liquid nitrogen. A 2.35Å dataset was collected at beamline 8-2 at the Advanced Light Source and processed using HKL3000[36].

Structure Determination and Refinement

The IL-15 quaternary complex structure was solved by molecular replacement using individual IL-2Rβ and γ_c subunits from PDB 2B5I and the IL-15—IL-15Rα complex from PDB 2Z3Q. Structural refinement was performed using the program PHENIX[37] and model adjustment carried out in COOT[38]. Bulk solvent flattening was used for solvent correction. For the initial refinement, rigid body, coordinate, and real-space refinement were employed with individual ADP refinement. TLS refinement was added in later refinement iterations.

Buried surface area calculations were performed with the Protein Interfaces, Surfaces, and Assemblies (PISA) server (http://www.ebi.ac.uk/msd-srv/prot_int/pistart.html)[39].

Simulations and Markov State Model (MSM)

Molecular dynamics simulations were run with Gromacs 4.5.2[40] using the AMBER03 force field[41]. Each structure was placed in a dodecahedral box of about 6.6 by 6.6 by 4.7 nm and solvated with approximately 6,250 tip3p water molecules. Conformations were first minimized with a steepest descent algorithm using a tolerance of 1000 kJ/mol/nm and a step size of 0.01 nm. A 1 nm cutoff was used for Coulombic and Van der Waals interactions and a grid-based neighbor list. Conformations were then equilibrated at 300 K and 1 bar by holding protein atoms fixed and allowing the surrounding water to relax for 500 ps with a 2 fs time-step. All bonds were constrained with the LINCS algorithm[42]. Center of mass motion was removed every step and a grid based neighbor list with a cutoff of 1.5 nm was updated every 10 steps. For electrostatics, we used fourth order PME[43] with a cutoff of 1.5 nm for Coulombic interactions, a Fourier spacing of 0.08 nm, and a tolerance of 1e-5. A hard cutoff of 1.2 nm was used for Van der Waals interactions with a switch starting at 1 nm. The temperature was controlled with the v-rescale thermostat[44] applied to the protein and solvent respectively with a time constant of 0.5 ps. The pressure was controlled with an isotropic Berenson barostat[45] applied to the entire system with a time constant of 0.5 ps and a compressibility of 4.5e-5 bar^{-1}. Long-range corrections were applied to energy and pressure. Production simulations up to 65 ns in length used the same parameters as for equilibration, with the exception that the protein atoms were no longer held fixed.

We used MSMBuilder[27] to construct an MSM with a 1 ns lag time. Based on previous work on protein folding[46], we chose to create 208 clusters (microstates) using a hybrid k-centers/k-medoids algorithm and the RMSD between pairs of conformations. All C_α and C_β atoms were used for the RMSD. Thermodynamic and kinetic properties were extracted from the MSM's eigenvalues and eigenvectors[47,48].

Assignments of residues to structural units used in RMSD plots are given in Supplementary Table 1. As in the MSM, all C_α and C_β atoms were used for these RMSDs.

Surface Plasmon Resonance (SPR)

SPR experiments were conducted on a Biacore T100 instrument at 25°C. Protein concentrations were quantified by UV spectroscopy at 280 nm using a Nanodrop2000 spectrometer (Thermo Scientific). Experiments were performed on a Biacore SA sensor chip (GE Healthcare), which was used to capture biotinylated IL-2Rβ (Rmax ~ 80 R.U.). To

control for non-specific binding, an unrelated biotinylated protein was immobilized with matching R.U. to the reference surface. Measurements were made using serial dilutions of IL-15 or IL-15—IL-15Rα complex in 1xHBS-P+ (GE Healthcare) supplemented with 0.01% BSA. IL-2Rβ surface was regenerated using 10 mM sodium acetate (pH 5.5) and 1 M $MgCl_2$. All data was analyzed using the Biacore T100 evaluation software version 2.0 with a 1:1 Langmuir binding model.

Mice

Animal protocols were approved by the NHLBI Animal Care and Use Committee and followed the NIH Guidelines "Using Animals in Intramural Research."

Cell Lines

YT-1 cells were maintained in complete RPMI 1640 medium (Gibco) in a humidified incubator at 37°C and 5% CO_2. IL-2Rα$^+$ YT-1 cells were obtained by enrichment with magnetic sorting (MACS) with PE-conjugated anti-IL-2Rα antibody (Biolegend) and anti-PE coated paramagnetic microbeads (Miltenyi Biotec). IL-2Rα enrichment was assessed by flow cytometry with the FL-2 channel using an Accuri C6 flow cytometer.

Phospho-flow Analysis of Intracellular STAT5 and ERK1-2 Signaling

For dose-response experiments, serial dilutions of IL-15, IL-15—IL-15Rα complex, IL-2, or H9 were applied to 2×10^5 IL-2Rα$^-$ or IL-2Rα$^+$ YT-1 cells per well in a 96-well plate. After 10 minutes, cells were fixed in paraformaldehyde and permeabilized in 100% methanol. For signaling kinetics experiments, 1 or 500 nM μM IL-15—IL-15Rα complex, IL-2, or H9 was applied to 2×10^5 YT cells/well and cells were fixed after the indicated time intervals (1, 2.5, 5, 15, 30, 60, or 120 minutes) and permeabilized with 100% methanol. Samples in methanol were multiplexed by fluorescent bar-coding[49] with amine-reactive DyLight 800 (Thermo Scientific) and Pacific Blue (Invitrogen) dyes and then stained with Alexa647-conjugated anti-STAT5 pY694 (BD Biosciences) and Alexa488-conjugated anti-ERK1-2 pT202/pY204 (Cell Signaling Technology). Mean cell fluorescence was determined with an LSRII flow cytometer. Dose-response and kinetic curves and EC_{50} values were calculated in GraphPad Prism.

CD8 Cell Isolation and Phospho-flow Analysis of Intracellular STAT5 and pS6K Signaling

Mouse CD8$^+$ T cells were isolated from spleens and lymph nodes of C57BL/6 mice using negative CD8 T-cell enrichment (CD8a$^+$ T cell Isolation kit II, Miltenyi Biotec). For 'freshly-isolated' cell cytokine stimulation assays, cells were used immediately. For generation of *in vitro* 'pre-activated' CD8$^+$ T cells, 6-well plates were pre-coated with 2 μg/ml of plate-bound anti-CD3 mAb (BD). CD8 cells were seeded at 1×10^6 cells/ml with 1 μg/ml of soluble anti-CD28 mAb (BD). Cells were cultured for 2 days with T-cell receptor stimulation, followed by 6 hours rest in fresh culture media.

For signaling kinetics experiments in freshly-isolated CD8$^+$ T-cells, 1 or 500 nM of IL-15, IL-15—IL-15Rα complex, IL-2, or H9 was applied to 2×10^5 CD8$^+$ T cells/well. For signaling kinetics experiments in pre-activated CD8$^+$ T-cells, 10 pM or 10 nM of IL-15, IL-15—IL-15Rα complex, IL-2, or H9 was used for stimulation. CD8$^+$ T cells were fixed

immediately after cytokine stimulation with PhosFlow Lyse/Fix buffer (BD) and then permeabilized by BD PhosFlow Perm Buffer III. Cells were then stained with PE-conjugated anti-STAT5 pY694 (BD Biosciences) and APC-conjugated anti-S6K pT389 (Cell Signaling Technology) at room temperature for 30 min in the dark. Data was acquired on a FACS Canto flow cytometer (BD Biosciences) and analyzed using FlowJo (Tree Star).

Receptor Internalization Experiments

500 nM IL-15, IL-15—IL-15Rα complex, IL-2, or H9 was applied to 2×10^5 YT cells in a 96-well plate at the indicated time intervals (1, 2.5, 5, 15, 30, 60, or 90 minutes) after which the cells were immediately transferred to ice to prevent further receptor internalization. Cells were washed twice with ice-cold FACS buffer (PBS + 0.5% BSA + 0.5 mM EDTA) and then stained with APC-conjugated anti-human IL-2Rβ (Biolegend) diluted 1:50, on ice for 30 minutes. Cells were washed twice more with ice-cold FACS buffer and then fixed with 1.5% paraformaldehyde in PBS for 10 minutes at room temperature. After fixation, mean cell fluorescence was determined with an Accuri C6 flow cytometer.

RNA-Seq Analysis

Splenic $CD8^+$ T cells were isolated from 6 week-old female C57BL/6 mice and treated with 1 nM or 500 nM of IL-2 or IL-15 for the indicated times, and total RNA was isolated. Three identically treated samples were pooled and cDNAs were synthesized using 2.5 ng of the pooled RNA and amplified by a two step PCR process (12 cycles with UP1 and UP2 primers (Supplementary Table 2) followed by 9 cycles with AUP1* and AUP2* primers (Supplementary Table 2) as described[50]. After fragmentation using a Bioraptor (Diagenode, Delville, NJ), 220-400 bp fragments were isolated using 2% E-Gel (Invitrogen), ends were repaired, adaptor (Illumina) was added using T4 DNA ligase (New England Biolabs), and amplified for 17 cycles using PE 1.0 and PE 2.0 primers (Illumina) and Phusion High Fidelity PCR Master Mix (New England Biolabs). The PCR products were barcoded (indexed) and sequenced on an Illumina HiSeq 2000 platform.

RNA-seq Data Analysis

Sequenced reads (single-end 36 bp) were aligned to the RefSeq mouse gene database (mm8 revision) with ELAND pipeline. Raw reads that fell on exons of each gene were counted and normalized RPKM values were calculated for each gene. Multidimensional scaling, linear regression modeling, and differential gene expression analysis were performed using statistical packages in R (www.r-project.org).

Gene expression analysis by real-time RT-PCR

cDNAs were synthesized using 200 ng of total RNA, oligo d[T], and Ominscript RT kit (Qiagen, Valencia, CA), and RT-PCR reactions were performed on an ABI 7900 HD Sequence Detection System using primers (Supplemental Table 2) and TaqMan 2x PCR Master mix (ABI/Ambion, Inc., Austin, TX). The relative expression levels were calculated based on the cycle number for *Rpl7*, as its expression level was constant under the experimental conditions.

Supplementary Material

Refer to Web version on PubMed Central for supplementary material.

Acknowledgments

The authors wish to thank E. Long, M. Rubinstein, and members of the Leonard and Garcia laboratories for helpful advice and discussions. The authors are particularly grateful to N. Goriatcheva, D. Waghray, and S. Fischer for technical assistance. This work was supported by NIH-RO1AI51321 (to K.C.G.), NIH R01-GM062868 (to V.S.P.), MRI-R2 (this award is funded under the American Recovery and Reinvestment Act of 2009 (Public Law 111-5)) (to V.S.P.), and the Division of Intramural Research, National Heart, Lung, and Blood Institute, NIH (W.J.L., J.X.L., P.L., S.M., and R.S.). A.M.R. was supported by the Stanford Medical Scientist Training Program (NIH-GM07365) and an NRSA award (NIH-F30DK094541). K.C.G. is an investigator of the Howard Hughes Medical Institute.

References

1. Waldmann TA. The biology of interleukin-2 and interleukin-15: implications for cancer therapy and vaccine design. Nat Rev Immunol. 2006; 6:595–601. [PubMed: 16868550]
2. Rochman Y, Spolski R, Leonard WJ. New insights into the regulation of T cells by gamma(c) family cytokines. Nat Rev Immunol. 2009; 9:480–490. [PubMed: 19543225]
3. Sneller MC, et al. IL-15 administered by continuous infusion to rhesus macaques induces massive expansion of CD8+ T effector memory population in peripheral blood. Blood. 2011; 118:6845–6848. [PubMed: 22067383]
4. Liao W, Lin JX, Leonard WJ. IL-2 family cytokines: new insights into the complex roles of IL-2 as a broad regulator of T helper cell differentiation. Curr Opin Immunol. 2011; 23:598–604. [PubMed: 21889323]
5. Wuest SC, et al. A role for interleukin-2 trans-presentation in dendritic cell-mediated T cell activation in humans, as revealed by daclizumab therapy. Nat Med. 2011; 17:604–609. [PubMed: 21532597]
6. Stonier SW, Schluns KS. Trans-presentation: a novel mechanism regulating IL-15 delivery and responses. Immunol Lett. 2010; 127:85–92. [PubMed: 19818367]
7. Marks-Konczalik J, et al. IL-2-induced activation-induced cell death is inhibited in IL-15 transgenic mice. Proc Natl Acad Sci U S A. 2000; 97:11445–11450. [PubMed: 11016962]
8. Syed RS, et al. Efficiency of signalling through cytokine receptors depends critically on receptor orientation. Nature. 1998; 395:511–516. [PubMed: 9774108]
9. Wang X, Rickert M, Garcia KC. Structure of the quaternary complex of interleukin-2 with its alpha, beta, and gammac receptors. Science. 2005; 310:1159–1163. [PubMed: 16293754]
10. Chirifu M, et al. Crystal structure of the IL-15-IL-15Ralpha complex, a cytokine-receptor unit presented in trans. Nat Immunol. 2007; 8:1001–1007. [PubMed: 17643103]
11. Walter TS, et al. Lysine methylation as a routine rescue strategy for protein crystallization. Structure. 2006; 14:1617–1622. [PubMed: 17098187]
12. LaPorte SL, et al. Molecular and structural basis of cytokine receptor pleiotropy in the interleukin-4/13 system. Cell. 2008; 132:259–272. [PubMed: 18243101]
13. Collins L, et al. Identification of specific residues of human interleukin 2 that affect binding to the 70-kDa subunit (p70) of the interleukin 2 receptor. Proc Natl Acad Sci U S A. 1988; 85:7709–7713. [PubMed: 3051003]
14. Eisenman J, et al. Interleukin-15 interactions with interleukin-15 receptor complexes: characterization and species specificity. Cytokine. 2002; 20:121–129. [PubMed: 12453470]
15. Pettit DK, et al. Structure-function studies of interleukin 15 using site-specific mutagenesis, polyethylene glycol conjugation, and homology modeling. J Biol Chem. 1997; 272:2312–2318. [PubMed: 8999939]
16. Zurawski SM, et al. Definition and spatial location of mouse interleukin-2 residues that interact with its heterotrimeric receptor. EMBO J. 1993; 12:5113–5119. [PubMed: 8262055]

17. Boulanger MJ, Bankovich AJ, Kortemme T, Baker D, Garcia KC. Convergent mechanisms for recognition of divergent cytokines by the shared signaling receptor gp130. Molecular Cell. 2003; 12:577–589. [PubMed: 14527405]
18. McFarland BJ, Strong RK. Thermodynamic analysis of degenerate recognition by the NKG2D immunoreceptor: not induced fit but rigid adaptation. Immunity. 2003; 19:803–812. [PubMed: 14670298]
19. Dubois S, Mariner J, Waldmann TA, Tagaya Y. IL-15Ralpha recycles and presents IL-15 In trans to neighboring cells. Immunity. 2002; 17:537–547. [PubMed: 12433361]
20. Hanick NA, et al. Elucidation of the interleukin-15 binding site on its alpha receptor by NMR. Biochemistry. 2007; 46:9453–9461. [PubMed: 17655329]
21. Mortier E, et al. Soluble interleukin-15 receptor alpha (IL-15R alpha)-sushi as a selective and potent agonist of IL-15 action through IL-15R beta/gamma. Hyperagonist IL-15 x IL-15R alpha fusion proteins. J Biol Chem. 2006; 281:1612–1619. [PubMed: 16284400]
22. Rubinstein MP, et al. Converting IL-15 to a superagonist by binding to soluble IL-15R{alpha}. Proc Natl Acad Sci U S A. 2006; 103:9166–9171. [PubMed: 16757567]
23. Rickert M, Wang X, Boulanger MJ, Goriatcheva N, Garcia KC. The structure of interleukin-2 complexed with its alpha receptor. Science. 2005; 308:1477–1480. [PubMed: 15933202]
24. Levin AM, et al. Exploiting a natural conformational switch to engineer an interleukin-2 ‘superkine’. Nature. 2012; 484:529–533. [PubMed: 22446627]
25. Balasubramanian S, et al. Ligand binding kinetics of IL-2 and IL-15 to heteromers formed by extracellular domains of the three IL-2 receptor subunits. Int Immunol. 1995; 7:1839–1849. [PubMed: 8580082]
26. Thanos CD, Randal M, Wells JA. Potent small-molecule binding to a dynamic hot spot on IL-2. J Am Chem Soc. 2003; 125:15280–15281. [PubMed: 14664558]
27. Bowman GR, Huang X, Pande VS. Using generalized ensemble simulations and Markov state models to identify conformational states. Methods. 2009; 49:197–201. [PubMed: 19410002]
28. Zambricki E, et al. Signaling T-cell survival and death by IL-2 and IL-15. Am J Transplant. 2005; 5:2623–2631. [PubMed: 16212621]
29. Castro I, Yu A, Dee MJ, Malek TR. The basis of distinctive IL-2- and IL-15-dependent signaling: weak CD122-dependent signaling favors CD8+ T central-memory cell survival but not T effector-memory cell development. J Immunol. 2011; 187:5170–5182. [PubMed: 21984699]
30. Cornish GH, Sinclair LV, Cantrell DA. Differential regulation of T-cell growth by IL-2 and IL-15. Blood. 2006; 108:600–608. [PubMed: 16569767]
31. Lindemann MJ, Hu Z, Benczik M, Liu KD, Gaffen SL. Differential regulation of the IL-17 receptor by gammac cytokines: inhibitory signaling by the phosphatidylinositol 3-kinase pathway. J Biol Chem. 2008; 283:14100–14108. [PubMed: 18348982]
32. Demirci G, Li XC. IL-2 and IL-15 exhibit opposing effects on Fas mediated apoptosis. Cell Mol Immunol. 2004; 1:123–128. [PubMed: 16212899]
33. Krieg C, Letourneau S, Pantaleo G, Boyman O. Improved IL-2 immunotherapy by selective stimulation of IL-2 receptors on lymphocytes and endothelial cells. Proc Natl Acad Sci U S A. 2010; 107:11906–11911. [PubMed: 20547866]
34. Ahmadzadeh M, Rosenberg SA. IL-2 administration increases CD4+ CD25(hi) Foxp3+ regulatory T cells in cancer patients. Blood. 2006; 107:2409–2414. [PubMed: 16304057]
35. Bessard A, Sole V, Bouchaud G, Quemener A, Jacques Y. High antitumor activity of RLI, an interleukin-15 (IL-15)-IL-15 receptor alpha fusion protein, in metastatic melanoma and colorectal cancer. Mol Cancer Ther. 2009; 8:2736–2745. [PubMed: 19723883]
36. Minor W, Cymborowski M, Otwinowski Z, Chruszcz M. HKL-3000: the integration of data reduction and structure solution--from diffraction images to an initial model in minutes. Acta Crystallogr D Biol Crystallogr. 2006; 62:859–866. [PubMed: 16855301]
37. Adams PD, et al. PHENIX: building new software for automated crystallographic structure determination. Acta Crystallogr D Biol Crystallogr. 2002; 58:1948–1954. [PubMed: 12393927]
38. Emsley P, Cowtan K. Coot: model-building tools for molecular graphics. Acta Crystallogr D Biol Crystallogr. 2004; 60:2126–2132. [PubMed: 15572765]

39. Krissinel E, Henrick K. Inference of macromolecular assemblies from crystalline state. J Mol Biol. 2007; 372:774–797. [PubMed: 17681537]
40. Hess B, Kutzner C, van der Spoel D, Lindahl E. GROMACS 4: Algorithms for highly efficient, load-balanced, and scalable molecular simulation. J Chem Theory Comput. 2008; 4:435–447. [PubMed: 26620784]
41. Duan Y, et al. A point-charge force field for molecular mechanics simulations of proteins based on condensed-phase quantum mechanical calculations. J Comp Chem. 2003; 24:1999–2012. [PubMed: 14531054]
42. Hess B. P-LINCS: A parallel linear constraint solver for molecular simulation. J Chem Theory Comput. 2008; 4:116–122. [PubMed: 26619985]
43. Darden T, York D, Pedersen L. A smooth particle mesh Ewald potential. J Chem Phys. 1995; 103:3014–3021.
44. Bussi G, Donadio D, Parrinello M. Canonical sampling through velocity rescaling. J Chem Phys. 2007; 126
45. Berendsen HJC, Postma PM, van Gunsteren WF, DiNola A, Haak JR. Molecular dynamics with coupling to an external bath. J Chem Phys. 1984; 81:3684–3690.
46. Bowman GR, Beauchamp KA, Boxer G, Pande VS. Progress and challenges in the automated construction of Markov state models for full protein systems. J Chem Phys. 2009; 131:124101. [PubMed: 19791846]
47. Bowman GR, Huang X, Pande VS. Network models for molecular kinetics and their initial applications to human health. Cell Res. 2010; 20:622–630. [PubMed: 20421891]
48. Noe F, Fischer S. Transition networks for modeling the kinetics of conformational change in macromolecules. Curr Opin Struct Biol. 2008; 18:154–162. [PubMed: 18378442]
49. Krutzik PO, Nolan GP. Fluorescent cell barcoding in flow cytometry allows high-throughput drug screening and signaling profiling. Nat Methods. 2006; 3:361–368. [PubMed: 16628206]
50. Tang F, et al. RNA-Seq analysis to capture the transcriptome landscape of a single cell. Nature protocols. 2010; 5:516–535. [PubMed: 20203668]

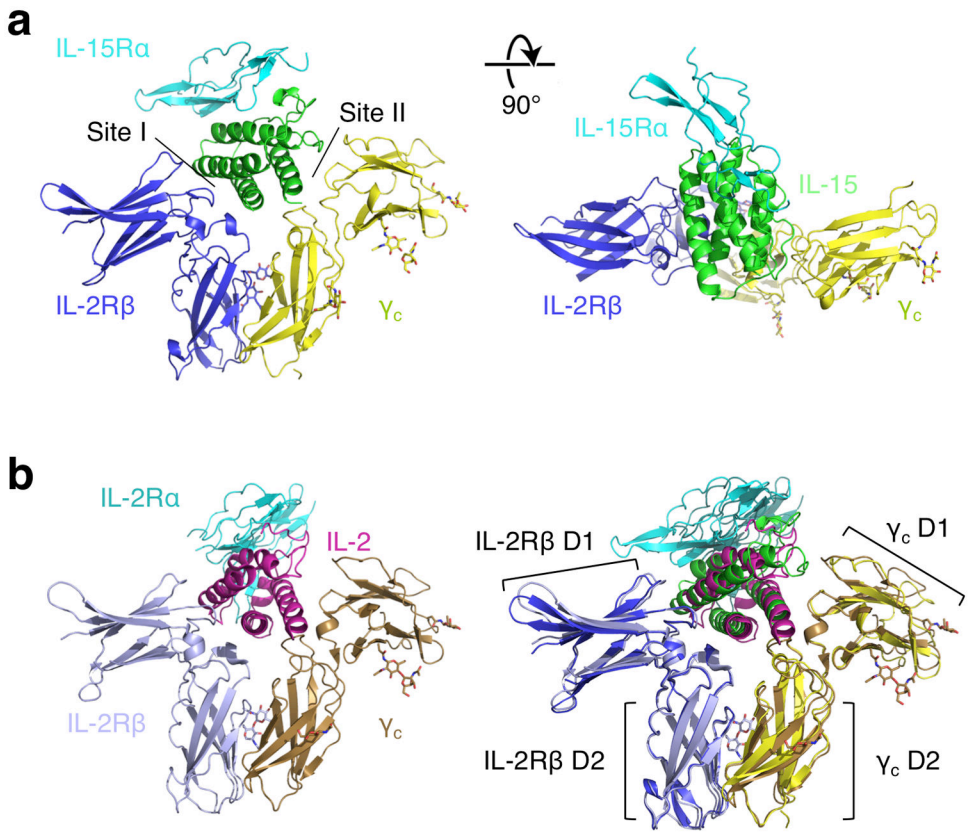

Figure 1.

The crystal structure of the quaternary IL-15 receptor complex. (**a**) Front (left) and top (right) views of the IL-15 quaternary receptor complex comprised of IL-15 (green), IL-15Rα (cyan), IL-2Rβ (blue), and γ_c (gold). The "site I" and "site II" interactions between IL-15 and IL-2Rβ and γ_c, respectively, are indicated. (**b**) The structure of the IL-2 quaternary complex (PDB code 2B5i; left) and the superimposition of the IL-15 and IL-2 receptor complexes (right). The IL-15 and IL-2 complexes superimpose with an r.m.s.d of 1.175Å)

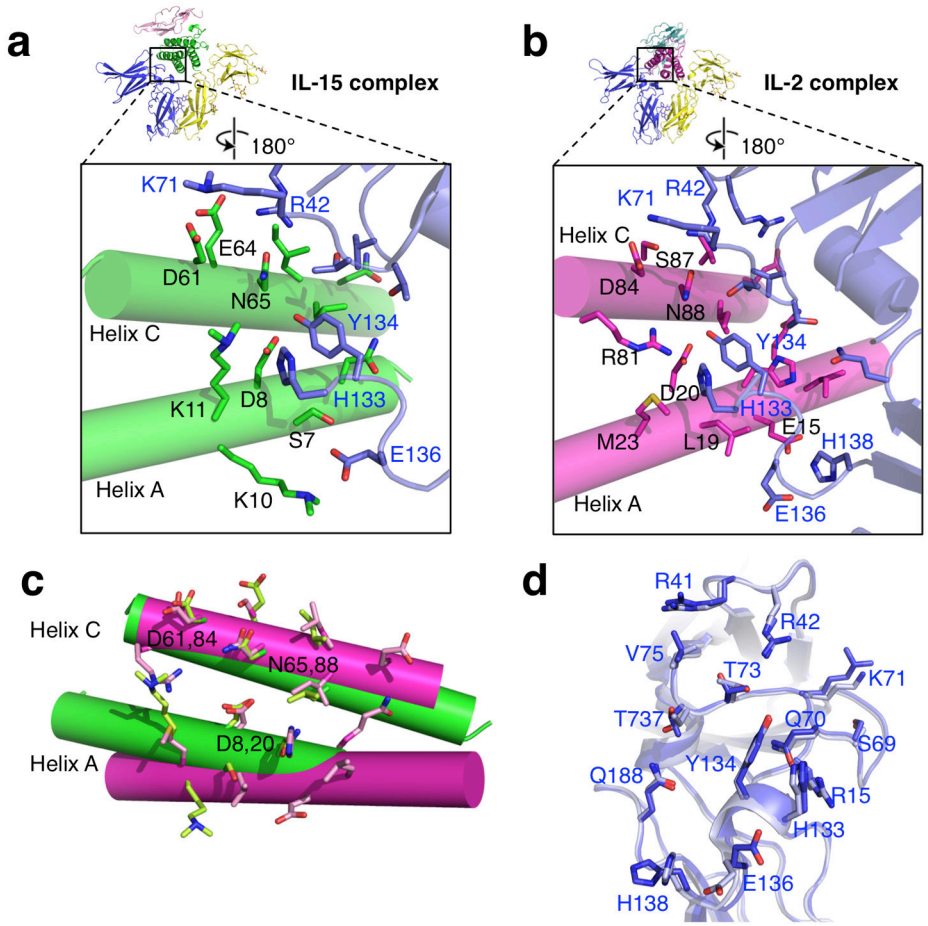

Figure 2.

Comparison of the IL-15 and IL-2 site I interfaces. (**a**) The site I interface of IL-15 (green cylinders and side chains) contacting IL-2Rβ (blue loops and side chains). (**b**) The site I interface of IL-2 (magenta cylinders and side chains) contacting IL-2Rβ (blue loops and side chains). (**c**) Superimposition of the IL-15 (green) and IL-2 (magenta) A and C helices showing structural conservation of D61, N65, and D8 of IL-15. (**d**) Superposition of IL-2Rβ bound to IL-15 (light blue) and IL-2 (blue) indicating the apparent rigidity of the interface in binding two distinct cytokines.

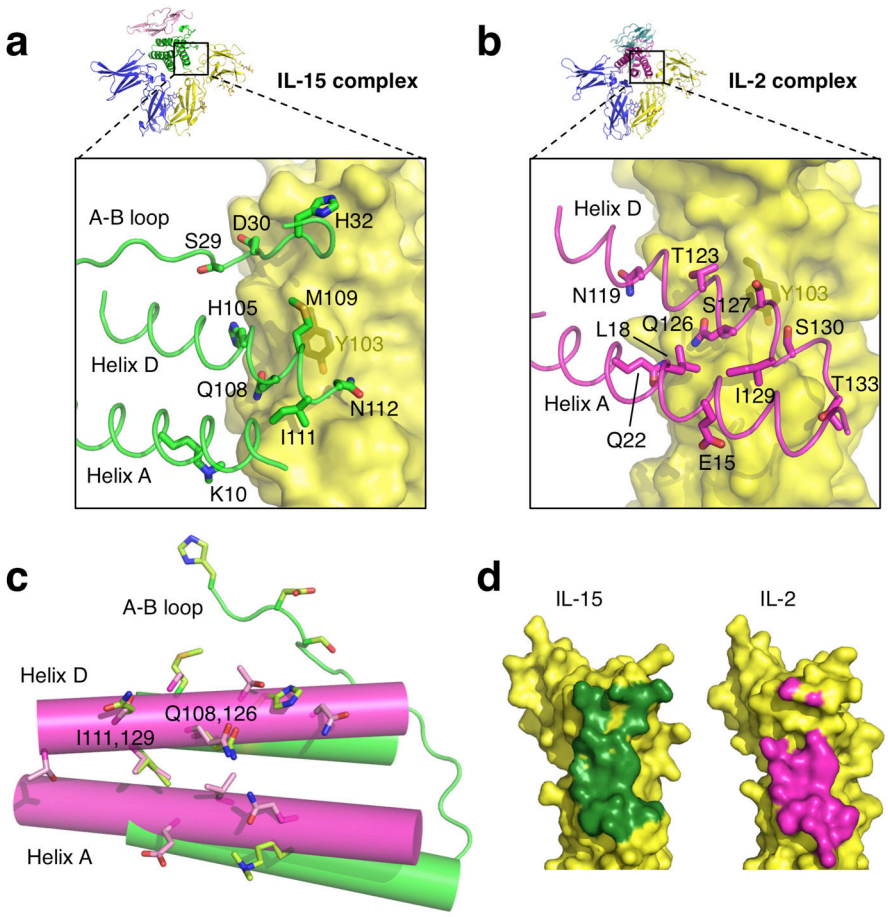

Figure 3.

Comparison of the IL-15 and IL-2 site II interfaces. (**a**) The site II interface of IL-15 (green tubes and side chains) binding to γ_c (yellow surface). X-SCID associated Y103 on γ_c is depicted in dark yellow. (**b**) The site II interface of IL-2 (magenta tubes and side chains) binding to γ_c (yellow surface). (**c**) Superimposition of the IL-15 (green) and IL-2 (magenta) A and D helices. Only Q108 and I111 of IL-15 are strictly conserved at the interface. (**d**) Comparison of γ_c binding interfaces. The surface of γ_c, shaded according to binding to IL-15 (left; dark green) or IL-2 (right; magenta). Note the increased contact area between IL-15 and γ_c, particularly in the upper part of the receptor.

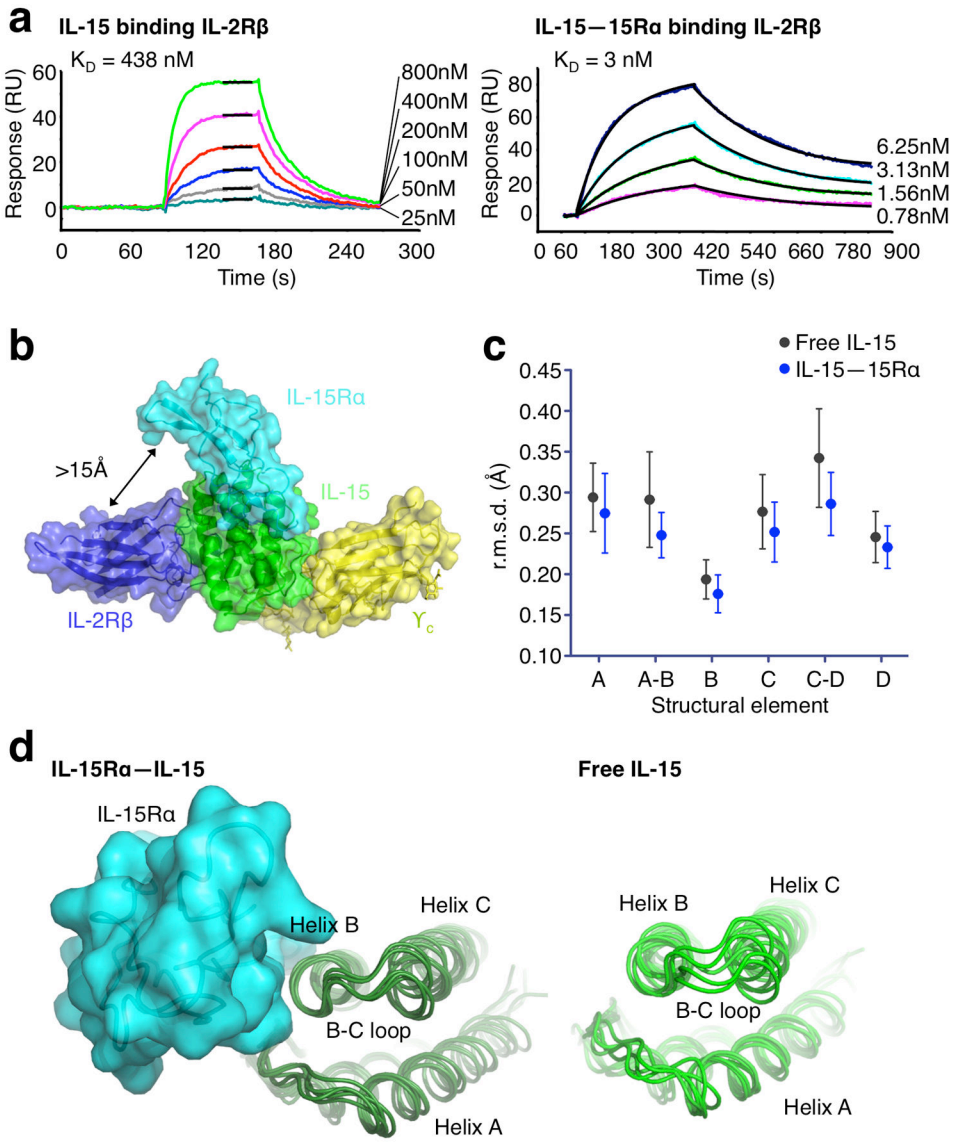

Figure 4.

Enhancement of IL-15—IL-2Rβ interaction by IL-15Rα. (**a**) SPR sensorgrams of IL-2Rβ binding to free IL-15 (left) or IL-15—IL-15Rα complexes (right) demonstrate IL-15—IL-15Rα complexes bind to IL-2Rβ with higher affinity (3 nM) relative to free IL-15 cytokine (438 nM). (**b**) Top view of the IL-15 quaternary complex indicating the lack of contact between IL-2Rβ and IL-15Rα. (**c**) A 65 ns molecular dynamics simulation shows a global reduction of the r.m.s.d. for each indicated structural element (assignments indicated in Supplementary Table 1) of IL-15 upon binding IL-15Rα. Error bars represent the standard error of r.m.s.d. (**d**) The five most highly-populated states of IL-15 bound to IL-15Rα (left) and free IL-15 (right) indicate the subtle global stabilization upon binding IL-15Rα.

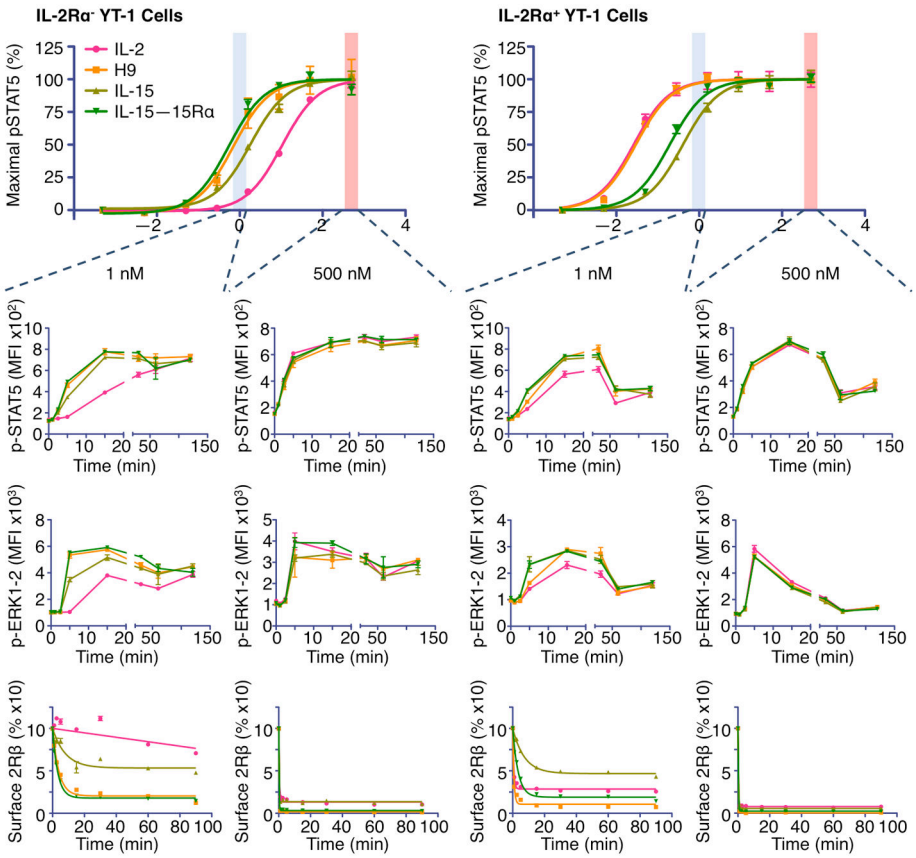

Figure 5.

Signaling analysis of IL-2 and IL-15 in YT-1 human NK cells. The phospho-STAT5 dose-response relationships for IL-2 (magneta circles), the "superkine" H9 (orange squares), IL-15 (light green upward triangles), and IL-15—IL-15Rα complexes (dark green downward triangles) are shown for IL-2Rα^{-} and IL-2Rα^{+} YT cells (top left and right, respectively). Signaling kinetics relationships for phospho-STAT5 (2nd row), phospho-ERK1/2 (3rd row), and IL-2Rβ receptor internalization (4th row) were determined at saturating (500 nM) and subsaturating (1 nM) concentrations (boxed columns). Differences in signaling amplitude and kinetics are concentration-dependent as cytokine signaling profiles converge at saturating concentrations. Error bars represent standard error of mean fluorescence intensity of samples in triplicate

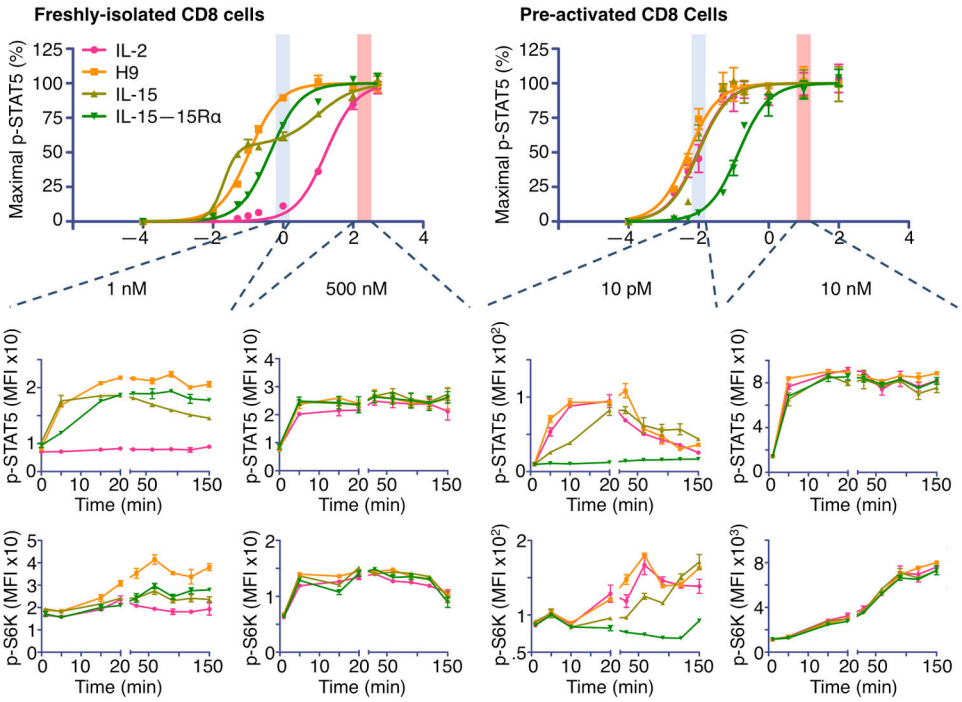

Figure 6.

Signaling analysis of IL-2 and IL-15 in primary mouse CD8 cells. As in Fig. 5, phospho-STAT5 dose-response relationships for IL-2 (magneta circles), H9 (orange squares), IL-15 (light green upward triangles), and IL-15—IL-15Rα complexes (dark green downward triangles) are shown for freshly-isolated CD8 T cells and CD8 T cells 'pre-activated' with anti-CD3 antibody. 'Pre-activated' cells express significantly higher levels of IL-2Rα and IL-15Rα than freshly-isolated cells (Supplementary Fig. 3b). Signaling kinetics relationships for phospho-STAT5 (2nd row) and phospho-S6kinase (3rd row) were determined at saturating (500 nM) and subsaturating (1 nM) concentrations (boxed columns). Similar to the effect of the cytokines in YT-1 cells, signaling amplitude and kinetics were readily predicted by the respective point where each cytokine resided on its dose-response relationship (top row). Error bars represent standard error of mean fluorescence intensity of samples in duplicate.

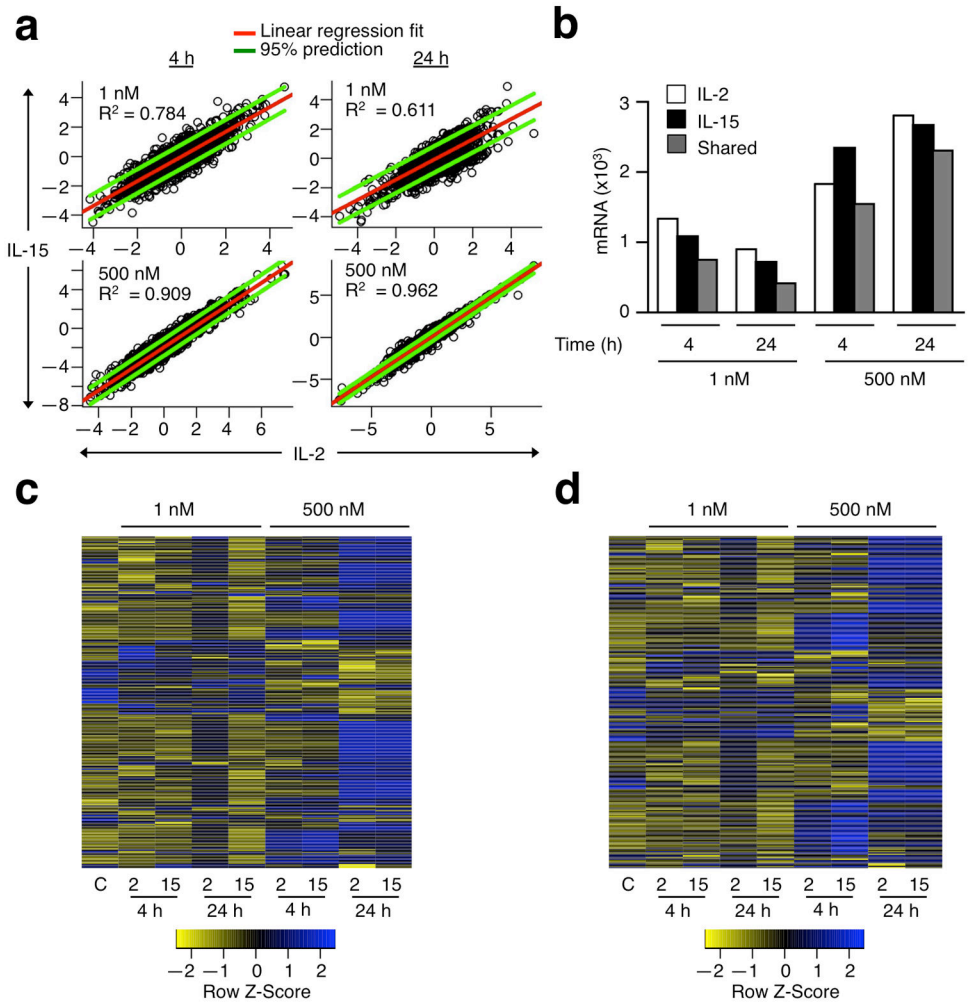

Figure 7.

RNA-seq analysis of gene transcription regulated by IL-2 and IL-15. (**a**) Correlations in fold changes (log2) of IL-2 and IL-15 regulated genes. 95% confidence intervals are not shown as they almost overlap with the 95% prediction from the linear regression fit. (**b**) Bar graphs showing the numbers of genes that are regulated by IL-2 or IL-15 at the indicated times and concentrations. (**c**) and (**d**) Heatmaps showing genes that are preferentially regulated by (**c**) IL-2 or (**d**) IL-15. Expression of each gene is normalized to the same range [-2, 2] for color display.

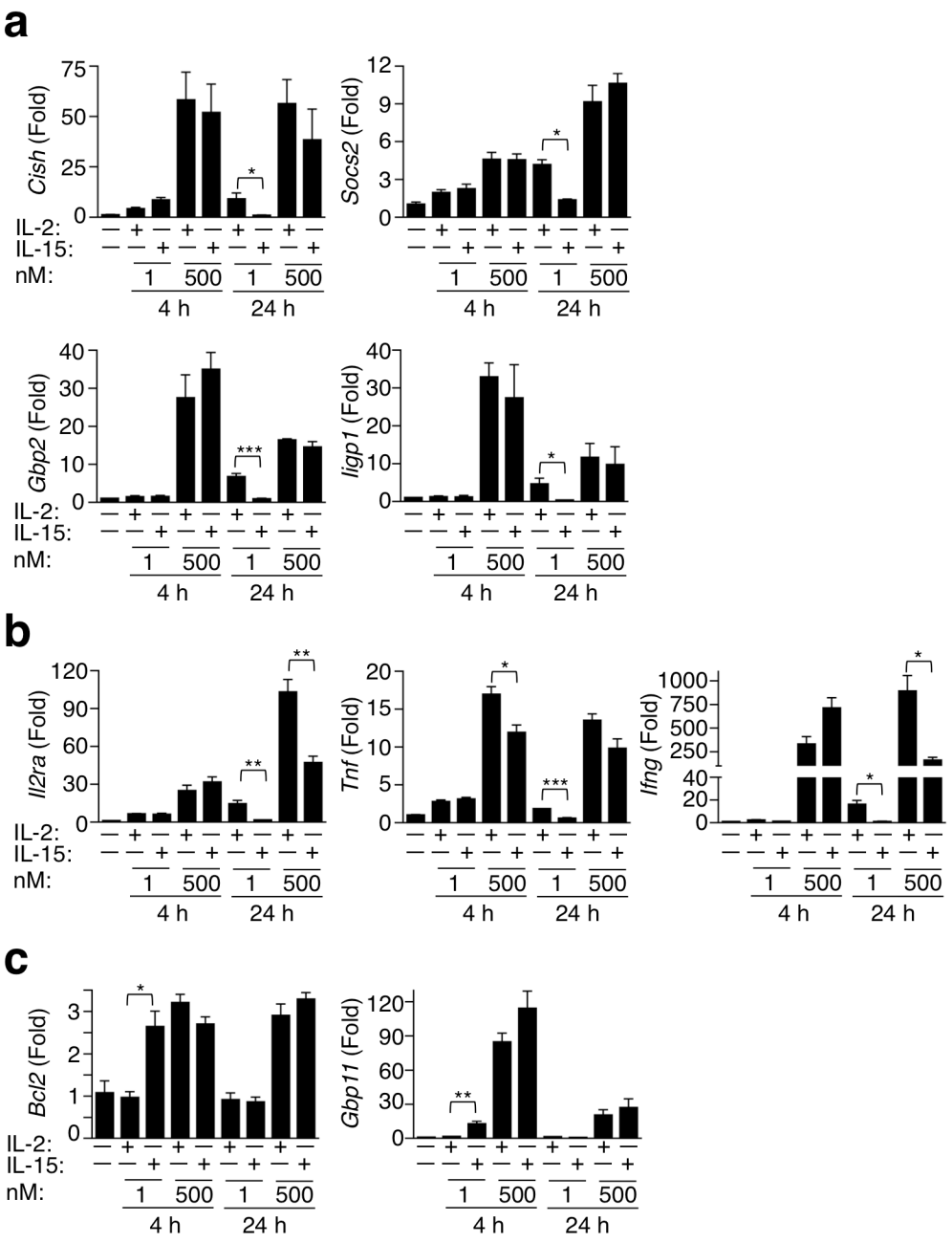

Figure 8.

qPCR validation of differentially regulated IL-2 and IL-15 target genes. (**a**) IL-2 and IL-15 induced expression of the indicated genes at 1 and 500 nM, at 4 and 24 hr time points. (**b**) Examples of genes more induced by IL-2 than IL-15 even at high dose. (**c**) Genes that are preferentially induced by IL-15 at low dose but similarly induced by IL-2 and IL-15 at high dose. The cDNA inputs were normalized based on the ΔCt values of *Rpl7* primers. Shown are the relative expression levels of triplicate samples of a representative experiment. * $p \leq 0.05$, ** $p \leq 0.01$, and *** $p \leq 0.001$.

Table 1

Data collection and refinement statistics

	IL-15—IL-15Rα—IL-2Rβ—γ_c complex
Data collection	
Space group	$P2_12_12_1$
Cell dimensions	
a, *b*, *c* (Å)	70.95, 74.61, 129.21
α, *β*, *γ* (°)	90.0, 90.0, 90.0
Resolution (Å)	40.23-2.35 (2.39-2.35)
R_{sym}	10.1 (65.6)
$I/\sigma I$	18.7 (2.3)
Completeness (%)	99.2 (94.9)
Redundancy	6.9 (5.5)
Refinement	
Resolution (Å)	40.23-2.35 (2.39-2.35)
No. reflections	29,215
R_{work}/R_{free}	19.2/24.3 (24.2/32.0)
No. atoms	
Protein	4,704
Ligand/ion	92
Water	235
B-factors	
Protein	40.3
Ligand/ion	53.3
Water	39.5
R.m.s deviations	
Bond lengths (Å)	0.004
Bond angles (°)	0.76

*Highest resolution shell is shown in parenthesis.